Wireless Over Cable In Femtocell Systems: A Case Study From Indoor Channel Measurements

J. Gambini[1], S. Savazzi[1], P. Castiglione[2], U. Spagnolini[1], G. Matz[3]
[1]Politecnico di Milano, DEI, Milan, I-20133 Italy. [2]FTW. Wien, Donau-City-Strasse 1, A-1220 Wien, Austria
[3]INTHFT, Vienna University of Technology Gusshausstrasse 25/389, A-1040 Vienna, Austria
e-mail: (gambini, savazzi, spagnoli)@elet.polimi.it, castiglione@ftw.at, gerald.matz@nt.tuwien.ac.at

***Abstract*— In this paper we consider a specific case-study where M indoor femtocells share the same radio resources for communicating to the central office. An outdoor macro-cell base station increases the level of co-channel interference (cross-tier interference). Analysis of the co-tier (arising from neighboring femtocells) and cross-tier interference levels affecting the multi-femtocell communications is based on a site-specific multi-link channel model obtained from a radio measurement campaign carried out at 2.4GHz [3]. In this context, we investigate the benefits of the Wireless over Cable (FemtoWoC) paradigm, based on the concept of deferring the PHY/MAC functionalities to a remote multicell FAP (femtocell access point), while leaving to the in-home device only the analog RF processing (amplify-and-forward -AF). Based on site-specific indoor-to-indoor and outdoor-to-indoor propagation parameters, interference mitigation for the uplink is carried out at the remote multicell FAP by taking into account realistic settings where: *i)* indoor radio propagation is impaired by Rician fading due to static multi-path fading components; *ii)* communication over the cable is affected by crosstalk produced by alien xDSL services; *iii)* imperfect knowledge of the radio channel limits the interference rejection performance at the multicell FAP.**

I. Introduction

The issue of centralized interference mitigation addressed by Network MIMO paradigm [1] can be tailored to the femtocell setting using a wireless-over-cable architecture for femtocells (*FemtoWoC architecture* [2] [10]) as illustrated in Fig. 1. The new paradigm relies on the Network MIMO principle as it is based on the concept of centralizing the PHY/MAC functionalities for multiple devices to a remote multicell Femtocell Access Point (multicell FAP), while leaving to the in-home devices only the analog radio frequency (multicell processing). This is attractive compared to conventional femtocells, since every home FAP is replaced by a simple amplify-and-forward (AF) relay device that interfaces the radio environment with the available cable infrastructure. The wired network can be based either on copper lines (e.g., telephone lines) or optical fibers. The amplified signals are forwarded to/from the remote multicell FAP, so as to exploit the concept of centralized multicell processing for reducing co/cross-tier interference.

A specific case-study is considered in this paper as depicted at the top of Fig. 1: M indoor femtocells and one outdoor macro-cell sharing the same spectrum. For uplink communication M femtocell users are delivering data towards indoor relays over indoor-to-indoor (I2I) links, and all the relays forward data over the cable interface towards the remote multicell FAP. Femtocells and macro-cells coexist in the same spectral resource so that RF interference mitigation becomes mandatory. Interference terms can be *co-tier* (originated by indoor neighboring femtocells) and *cross-tier* (macrocell-to-femtocell and vice-versa). In this work, analysis of the co-tier and cross-tier interference levels observed by the femtocell users is based on a site-specific multi-link channel model obtained from a radio indoor measurement campaign carried out at 2.4GHz [3]. The purpose is to provide a tunable "software test-bed" for assessing interference mitigation policies tailored to the femtocell setting.

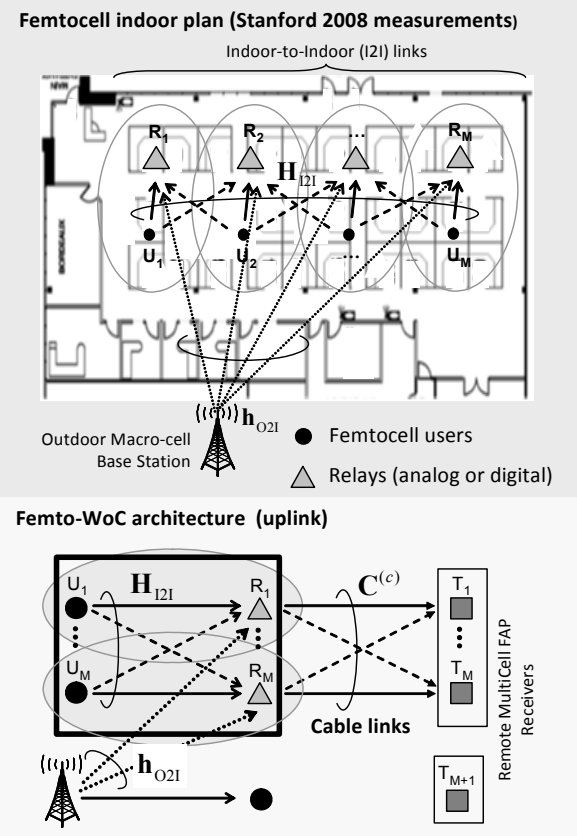

Fig. 1: Radio propagation for indoor femtocells. Indoor-to-indoor (I2I) and outdoor-to-indoor (O2I) wireless channel parameters are taken from a 2.4GHz measurement campaign (Stanford, 2008).

The work of P. Castiglione and G. Matz was supported by the Austria Science Fund (FWF) through grant NFN SISE (S106).

The uplink baseband system model for the FemtoWoC architecture [2] employing orthogonal frequency division multiple access (OFDMA) is reviewed in Sec. II. Channel and interference modeling for the wireless interface based on 2.4GHz measurements [3] is detailed in Sec. III. Benefits of the FemtoWoC architecture are investigated in Sec. IV-V by focusing on different system topologies/interference scenarios for both the wireless and the cable environment. The impact of imperfect knowledge of the radio channel is also discussed. Conclusions follow in Sec. VI.

II. System Model

In what follows, we review the FemtoWoC system model for the uplink [2]. Let us consider the system in Fig. 1, where M femtocells are connected to a common remote multicell FAP via M twisted pair telephone lines deployed in the same cable bundle, each having length d_i. The remote multicell FAP consists of M transceivers $\{T_i\}_{i=1}^{M}$. Each femtocell encompasses a single AF relay R_i serving one user U_i. The femtocell users $\{U_i\}_{i=1}^{M}$ share the same spectrum, thus creating a compound $M \times M$ multiple-input-multiple-output (MIMO) system composed of the cascade of a wireless MIMO channel connecting to the AF relays $\{R_i\}_{i=1}^{M}$, and a cable MIMO channel to the M transceivers $\{T_i\}_{i=1}^{M}$. Each AF relay is in charge of performing a frequency conversion of the RF wireless signals received from the M femtocell users to band-pass signals that are suitable for the cable interface. Modulation is based on orthogonal frequency division multiplexing (OFDM) using K subcarriers.

Let $\mathbf{s}_k = [s_{1,k},\, s_{2,k},\, ...,\, s_{M,k}]^T$ denote the set of frequency domain symbols transmitted by the M femtocell users over the kth OFDM subcarrier. The symbol time index is neglected to simplify the notation. We assume that all the users transmit with the same power over all the K subcarriers, such that $E[|s_{i,k}|^2] = P_T$. Assuming that all the end-to-end links $U_i \rightarrow T_i$ are simultaneously active, the discrete-time baseband signals received by the M relay nodes over the kth subcarrier $\mathbf{z}_k = [z_{1,k}, ..., z_{M,k}]^T$ of the wireless interface (first hop) is

$$\mathbf{z}_k = \mathbf{H}_{\mathrm{I2I},k}\mathbf{s}_k + \mathbf{h}_{\mathrm{O2I},k}s_{BS,k} + \mathbf{n}_k, \tag{1}$$

where $\mathbf{H}_{\mathrm{I2I},k}$ is the $M \times M$ MIMO wireless channel that models the indoor-to-indoor (I2I) links between the femtocell users and the AF relay nodes, i.e. $\{\mathbf{H}_{\mathrm{I2I},k}\}_{i,j} = h_{U_j \rightarrow R_i,k}$; the term $\mathbf{n}_k \sim \mathcal{CN}(\mathbf{0}, N_{0,k}\mathbf{I})$ is the additive noise over the kth RF subcarrier, and the vector $\{\mathbf{h}_{\mathrm{O2I},k}\}_i = h_{BS \rightarrow R_i,k}$ models the additional outdoor-to-indoor (O2I) fading impairments originated by an outdoor macro-cell BS transmitting with power $E[|s_{BS,k}|^2] = P_{BS}$ and operating over the same frequency spectrum. Each ith relay node overhears the analog signal over the wireless interface, amplifies every received symbol $z_{i,k}$ by a factor $a_{i,k}$ to ensure that $\mathrm{E}[|a_{i,k}z_{i,k}|^2] = P_R$ (only depending on the long-term statistics of the radio channels), and re-transmits it over the cable interface by translating the symbol over the corresponding cable subcarrier. Let $\mathbf{C}_k$ denote the $M \times M$ cable MIMO channel that models attenuation $[\mathbf{C}_k]_{ii} = c_{R_i \rightarrow T_i,k}$ and cross-talk $[\mathbf{C}_k]_{ij} = c_{R_j \rightarrow T_i,k}$, $i \neq j$, at subcarrier k. Furthermore, let us define the diagonal matrix $\mathbf{A}_k = \mathrm{diag}(a_{1,k}, ..., a_{M,k})$ that contains the relay amplitude gains $\{a_{i,k}\}_{i=1}^{M}$. The $M \times 1$ baseband signal received by the remote multicell FAPs transceivers over the kth subcarrier (of the cable interface) is

$$\begin{aligned} \mathbf{y}_k &= \mathbf{C}_k\mathbf{A}_k\mathbf{z}_k + \mathbf{n}_k^{(c)} \\ &= \underbrace{\tilde{\mathbf{C}}_k\mathbf{H}_{\mathrm{I2I},k}\mathbf{s}_k}_{\mathbf{Q}_{\mathrm{I2I},k}\times\mathbf{s}_k} + \underbrace{\tilde{\mathbf{C}}_k\mathbf{h}_{\mathrm{O2I},k}s_{BS,k}}_{\mathbf{n}_{\mathrm{O2I},k}} + \underbrace{\tilde{\mathbf{C}}_k\mathbf{n}_k + \mathbf{n}_k^{(c)}}_{\tilde{\mathbf{n}}_k}. \end{aligned} \tag{2}$$

Here, $\tilde{\mathbf{C}}_k = \mathbf{C}_k\mathbf{A}_k$, and $\mathbf{n}_k^{(c)} \sim \mathcal{CN}(\mathbf{0}, N_{0,k}^{(c)}\mathbf{I})$ with $\{\mathbf{n}_k^{(c)}\}_i = n_{T_i,k}^{(c)}$ is the additive noise over the kth subcarrier that accounts for both the cable-specific thermal noise and the alien crosstalk [4] produced by other xDSL services possibly deployed in the same cable binder. The compound MIMO channel $\mathbf{Q}_{\mathrm{I2I},k} = \tilde{\mathbf{C}}_k\mathbf{H}_{\mathrm{I2I},k}$ combines the wireless and the wired MIMO channel interfaces. Furthermore, $\mathbf{n}_{\mathrm{O2I},k}$ denotes cross-tier O2I interference with covariance matrix $\mathrm{E}[\mathbf{n}_{\mathrm{O2I},k}\mathbf{n}_{\mathrm{O2I},k}^H] = \mathbf{R}_{\mathrm{O2I},k} = P_{BS}\tilde{\mathbf{C}}_k\mathrm{E}[\mathbf{h}_{\mathrm{O2I},k}\mathbf{h}_{\mathrm{O2I},k}^H]\tilde{\mathbf{C}}_k^H$. The equivalent noise term is $\tilde{\mathbf{n}}_k \sim \mathcal{CN}(\mathbf{0}, \mathbf{R}_k)$, with $\mathbf{R}_k = N_{0,k}\tilde{\mathbf{C}}_k\tilde{\mathbf{C}}_k^H + N_{0,k}^{(c)}\mathbf{I}$.

III. Indoor Channel Modeling

In this section, we describe the wireless multi-link channel model for the femtocell environment derived from experimental measurements [3]. The model encompasses both the indoor-to-indoor (I2I) and outdoor-to-indoor (O2I) radio links, and describes the statistics of fading over each sub-carrier. The channel modeling for the cable interface follows ref. [5], and it is not described in detail due to lack of space.

The wireless multi-link channel model is based on real point-to-point radio channel measurements [3] carried out in an office environment at 2.4 GHz. Despite the absence of the Line-Of-Sight path, the wireless I2I/O2I terms $h_{U_i \rightarrow R_j,k}$ and $h_{BS \rightarrow R_j,k}$ are affected by Rician fading. Moreover, they are assumed constant over the whole symbol, while they are continuously varying from symbol to symbol. Rician K-factor arises from the static multipath fading component as described in the following.

I2I channels $\mathbf{H}_{\mathrm{I2I},k}$*:* Let $g_{U_i \rightarrow R_j,k} = -[\mathrm{E}\{|h_{U_i \rightarrow R_j,k}|^2\}]_{\mathrm{dB}}$ be the path loss in dB and $K_{U_i \rightarrow R_j,k} = [|E\{h_{U_i \rightarrow R_j,k}\}|^2]_{\mathrm{dB}} - [\mathrm{var}\{h_{U_i \rightarrow R_j,k}\}]_{\mathrm{dB}}$ the Rician K-factor experienced by the I2I link (U_i, R_j) with distance $D_{U_i \rightarrow R_j}$; these parameters are modeled as

$$\begin{aligned} g_{U_i \rightarrow R_j,k} &= g_0^{\mathrm{I2I}} + \alpha_{\mathrm{I2I}}\left[D_{U_i \rightarrow R_j}/D_{\mathrm{In}}\right]_{\mathrm{dB}} \\ &\quad + \tilde{g}_{U_i \rightarrow R_j} - \left[|\tilde{r}_k|^2\right]_{\mathrm{dB}} + N_{U_i,R_j}^{\mathrm{wall}}g_{\mathrm{Wall}}, \\ K_{U_i \rightarrow R_j,k} &= K_0^{\mathrm{I2I}} - \kappa_{\mathrm{I2I}} \times \left[D_{U_i \rightarrow R_j}/D_{\mathrm{In}}\right]_{\mathrm{dB}} + \tilde{K}_{U_i \rightarrow R_j,k}, \end{aligned} \tag{3}$$

where $g_0^{\mathrm{I2I}} = 40.4\mathrm{dB}$ (the reference deterministic free space loss at $D_{\mathrm{In}} = 1\mathrm{m}$), $K_0^{\mathrm{I2I}} = 16.9\mathrm{dB}$, the indoor path loss exponent is $\alpha_{\mathrm{I2I}} = 1.75$, and the indoor K-factor exponent is $\kappa_{\mathrm{I2I}} = 0.53$. The loss of the walls obstructing the link (U_i, R_j) is modeled by the product term $N_{U_i,R_j}^{\mathrm{wall}}g_{\mathrm{Wall}}$, where the typical value $g_{\mathrm{Wall}} = 3 \div 22\mathrm{dB}$ [6]. Notice that the presence of the walls does not affect the static component $K_{U_i \rightarrow R_j,k}$. Random deviations from nominal values for path-loss and K-factor, e.g. caused by obstructions, are $\tilde{g}_{U_i \rightarrow R_j} \sim \mathcal{N}(0, 4.4\mathrm{dB})$ and $\tilde{K}_{U_i \rightarrow R_j,k} \sim \mathcal{N}(0, 5.9\mathrm{dB})$. The term $\tilde{r}_k \sim \mathcal{N}(0,1)$ accounts

for the additional Rayleigh distributed static multipath fading component.

O2I interference channel $\mathbf{h}_{\mathrm{O2I},k}$*:* The model for the O2I fading interference term $h_{BS\to R_j,k}$ conforms with the O2I urban micro-cell scenario B4 in [6]. The propagation is modeled as the combination of three main contributions: the outdoor propagation from the BS to the nearest wall (superscript Out), the propagation through the wall and the indoor propagation from the wall to the femtocell user (superscript In). The path loss $g_{BS\to R_j,k} = -[E\{|h_{BS\to R_j,k}|^2\}]_{\mathrm{dB}}$ and the Rician K-factor $K_{BS\to R_j,k} = [|E\{h_{BS\to R_j,k}\}|^2]_{\mathrm{dB}} - [\mathrm{var}\{h_{BS\to R_j,k}\}]_{\mathrm{dB}}$ thus equal

$$g_{BS\to R_j,k} = g^{\mathrm{Out}}_{BS\to R_j} + N^{\mathrm{wall}}_{BS\to R_j} g_{\mathrm{Wall}} + g^{\mathrm{In}}_{BS\to R_j,k}, \quad (4)$$

$$K_{BS\to R_j,k} = K^{\mathrm{Out}}_{BS\to R_j} + K^{\mathrm{In}}_{BS\to R_j,k} \quad (5)$$

where $N^{\mathrm{wall}}_{BS\to R_j}$ accounts for number of walls encountered by the outdoor interferer signal towards the relay R_j. The outdoor parameters $(g^{\mathrm{Out}}_{BS\to R_j}, K^{\mathrm{Out}}_{BS\to R_j})$ are modeled as in (3), where distance is now measured between the BS and the outdoor wall. For outdoor propagation, the measured path-loss exponent is found as $\alpha_{\mathrm{O2I}} = 3.8$, while $\kappa_{\mathrm{I2I}} = 0.45$. The indoor terms $(g^{\mathrm{In}}_{BS\to R_j,k}, K^{\mathrm{In}}_{BS\to R_j,k})$ are taken from the scenario B4 in [6, Table 4-4] and from [3, (15)], respectively.

IV. MIMO Processing At Multicell-FAP

The user symbols $\mathbf{s}_k$ at the kth subcarrier are decoded at the remote multicell FAP via linear MIMO processing according to $\hat{\mathbf{s}}_k = \mathbf{W}_k\mathbf{y}_k$ with the $M \times M$ weight matrix $\mathbf{W}_k = [\mathbf{w}_{k,1}, ..., \mathbf{w}_{k,M}]^H$, where $\mathbf{w}_{k,i} \in \mathbb{C}^{M\times 1}$. The power of the desired signal then equals $\gamma_{U_i} = P_T|\mathbf{w}^H_{k,i}\mathbf{q}^{(i)}_{\mathrm{I2I},k}|^2$, where $\mathbf{q}^{(i)}_{\mathrm{I2I},k} = \tilde{\mathbf{C}}_k\mathbf{h}^{(i)}_{\mathrm{I2I},k}$ with $\mathbf{h}^{(i)}_{\mathrm{I2I},k}$ denoting the ith column of $\mathbf{H}_{\mathrm{I2I},k}$ and $\mathbf{q}^{(i)}_{\mathrm{I2I},k}$ denoting the ith column of $\mathbf{Q}_{\mathrm{I2I},k}$. The co-tier interference power is given by $\gamma_{U_{j\neq i}} = P_T\sum^M_{j=1,j\neq i}|\mathbf{w}^H_{k,i}\mathbf{q}^{(j)}_k|^2$ and the cross-tier interference (originating from the macro-cell BS) has power $\gamma_{BS} = |\mathbf{w}^H_{k,i}\mathbf{n}_{\mathrm{O2I},k}|^2$. The signal-to-interference-plus-noise ratio (SINR) for subcarrier k of user U_i follows from (2) as

$$\Gamma_{k,i} = \gamma_{U_i}/(\gamma_{U_{j\neq i}} + \gamma_{BS} + |\mathbf{w}^H_{k,i}\tilde{\mathbf{n}}_k|^2). \quad (6)$$

The linear minimum mean square error (LMMSE) detector for the compound (air+cable) MIMO channel reads

$$\mathbf{W}_k = \sqrt{P_T}\mathbf{Q}^H_{\mathrm{I2I},k}(P_T\mathbf{Q}_{\mathrm{I2I},k}\mathbf{Q}^H_{\mathrm{I2I},k} + \mathbf{R}_{\mathrm{O2I},k} + \mathbf{R}_k)^{-1}. \quad (7)$$

Average SINR $\bar{\Gamma}_{k,i} = \mathrm{E}_{\mathbf{H}_{\mathrm{I2I},k},\mathbf{h}_{\mathrm{O2I},k}}[\Gamma_{k,i}]$ over I2I and O2I fading impairments is chosen as the performance metric for analysis and it is numerically evaluated according to the multi-link channel modeling of Sec. III.

A. Modeling Of Channel Out-dating

The LMMSE detector defined in (7) assumes perfect knowledge of the compound MIMO channel matrix $\mathbf{Q}_{\mathrm{I2I},k}$ at the remote multicell FAP. In practical systems, an estimation of the MIMO matrix $\hat{\mathbf{Q}}_{\mathrm{I2I},k}$ is obtained at the remote FAP from known sequences of symbols (pilot symbols) that are periodically inserted over time (and frequency domain) according to a predefined bidimensional grid. The compound MIMO matrix

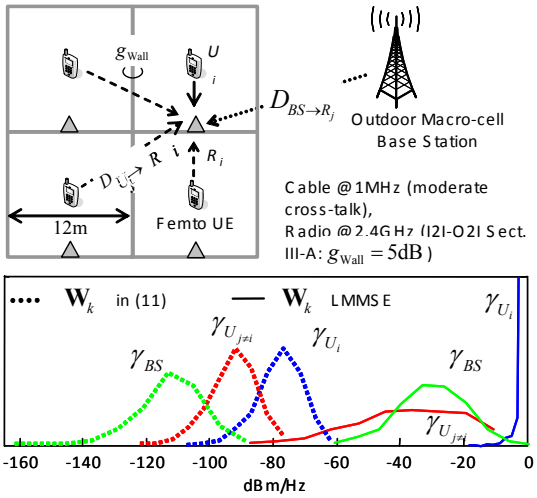

Fig. 2: Top: simulation setup. Bottom: probability density functions (pdfs) of useful signal power γ_{U_i}, co-tier interference power $\gamma_{U_{j\neq i}}$, and cross-tier interference power γ_{BS} at the multicell FAP. Pdfs are evaluated for the cable-MMSE case (dashed lines) and for network MIMO LMMSE processing (solid lines) from modeling of Sec. III (here with perfect channel state information).

$\mathbf{Q}_{\mathrm{I2I},k} = \tilde{\mathbf{C}}_k\mathbf{H}_{\mathrm{I2I},k}$ consists of terms that can be reasonably considered as static over a very large temporal scale (the cable interface $\tilde{\mathbf{C}}_k$) and of terms that are continuously time-varying over consecutive OFDM blocks (the radio interface $\mathbf{H}_{\mathrm{I2I},k}$). In this section we analyze the impact of the radio channel out-dating on the performance of the LMMSE detector at the multicell FAP, while the cable MIMO channel is assumed as known. The (unbiased) estimates of the compound channels are $\hat{\mathbf{q}}^{(i)}_{\mathrm{I2I},k} = \tilde{\mathbf{C}}_k\hat{\mathbf{h}}^{(i)}_{\mathrm{I2I},k}$, where channel out-dating is modeled according to the auto-regressive model

$$\mathbf{h}^{(i)}_{\mathrm{I2I},k} = \mathrm{diag}(\boldsymbol{\rho}_{U_i}) \times \hat{\mathbf{h}}^{(i)}_{\mathrm{I2I},k} + \boldsymbol{\Delta}\mathbf{h}^{(i)}_k, \quad (8)$$

with $[\boldsymbol{\Delta}\mathbf{h}^{(i)}_k]_j \sim \mathcal{CN}[0,(1-\rho^2_{U_i\to R_j})g_{U_i\to R_j}]$. The vector $\boldsymbol{\rho}_{U_i} = [\rho_{U_i\to R_j}]^M_{j=1}$ collects the correlations $\rho_{U_i\to R_j}$ that depend on the environment (e.g., the Doppler shift [12]) and on the interval among two successive training phases [7] for user U_i. Imperfect channel estimation (8) has the effect of modifying the SINR for subcarrier k of user U_i with respect to (6) as

$$\Gamma_{k,i} = \frac{\gamma_{U_i}}{\gamma_{U_{j\neq i}} + \Delta\gamma_{U_j} + \gamma_{BS} + |\hat{\mathbf{w}}^H_{k,i}\tilde{\mathbf{n}}_k|^2}, \quad (9)$$

where the LMMSE detector (7) is now based on the estimated compound channel $\hat{\mathbf{Q}}_{\mathrm{I2I},k}$. The power of the desired signal, the co-tier and the cross-tier interference become $\gamma_{U_i} = P_T|\hat{\mathbf{w}}^H_{k,i}\mathrm{diag}(\boldsymbol{\rho}_{U_i})\hat{\mathbf{q}}^{(i)}_{\mathrm{I2I},k}|^2$, $\gamma_{U_{j\neq i}} = P_T\sum^M_{j=1,j\neq i}\rho^2_j|\hat{\mathbf{w}}^H_{k,i}\mathrm{diag}(\boldsymbol{\rho}_{U_j})\hat{\mathbf{q}}^{(j)}_{\mathrm{I2I},k}|^2$ and $\gamma_{BS} = |\hat{\mathbf{w}}^H_{k,i}\mathbf{n}_{\mathrm{O2I},k}|^2$, respectively. Error term due to out-dating of radio channel is $\Delta\gamma_{U_j} = P_T \times \sum^M_{j=1}\left|\hat{\mathbf{w}}^H_{k,i}\tilde{\mathbf{C}}_k\boldsymbol{\Delta}\mathbf{h}^{(j)}_k\right|^2$. The new average SINR $\bar{\Gamma}_{k,i} = \mathrm{E}_{[\hat{\mathbf{h}}^{(i)}_{\mathrm{I2I},k},\boldsymbol{\Delta}\mathbf{h}^{(i)}_k]^M_{i=1},\mathbf{h}_{\mathrm{O2I},k}}[\Gamma_{k,i}]$ still conforms with the multi-link channel modeling of Sec. III.

V. Case Study In Indoor Environments

The purpose here is to highlight the benefits of MIMO processing for the uplink of the FemtoWoC architecture as de-

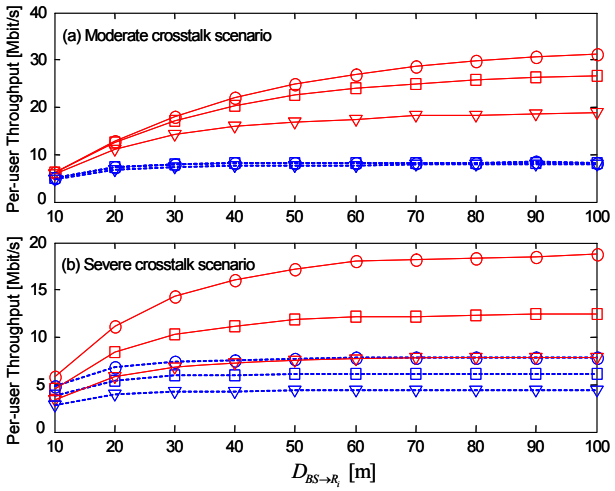

Fig. 3: Per-user LTE UL throughput versus the distance $D_{BS\to R_i}$ $\forall i$ for moderate (a) and severe (b) alien crosstalk scenario, and for LMMSE (solid lines) and cable-MMSE (dashed lines) MIMO processing ($g_{\text{Wall}} = 5$dB).

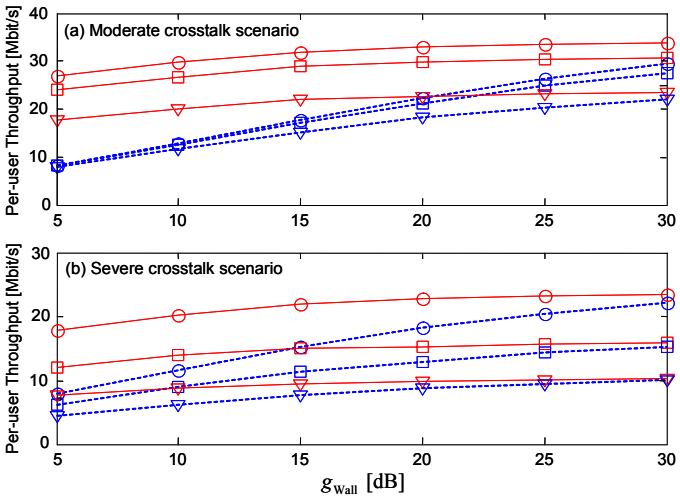

Fig. 4: Per-user LTE UL throughput versus the penetration loss g_{Wall}, (same legend and system parameters as in fig. 3, with the macrocell user distance selected as $D_{BS\longrightarrow R_i} = 60$m $\forall i$).

scribed in Sec. IV, assuming perfect channel knowledge. The impact of imperfect channel knowledge will be evaluated in the next section. The benefits of network MIMO are compared with a scenario (referred to as *cable-MMSE*) where the weight matrix $\mathbf{W}_k = \tilde{\mathbf{C}}_k^H(\tilde{\mathbf{C}}_k\tilde{\mathbf{C}}_k^H + N_{0,k}^{(c)}\mathbf{I})^{-1}$ only takes into account the cable MIMO channel, without any attempt to mitigate cross-tier and co-tier interference over the radio links. In order to simplify the model in fig. 1 (top), we focus on a block of 2×2 apartments of size 12m×12m deployed according to a square grid, and separated by walls with penetration loss g_{Wall} but using the same statistical properties derived in Sec. III. A femtocell is deployed in each apartment, and the AF relay and the femtocell user are positioned according to the regular structure as sketched in Fig. 2. The lengths $\{d_i\}_{i=1}^{M}$ of the backhauling copper cables have been randomly selected in the intervals [250 m, 350 m], [550 m, 650 m], or [850 m, 950 m] in order to model a short, medium, and long range, respectively [8].

LTE with 10MHz system bandwidth is simulated for the femtocell environment by following the guidelines in [9]. In the case study both the femtocell users and the macrocell interferer employ a transmit power of 20dBm, that is uniformly split over the sub-carriers. The RF noise floor is chosen to equal -162dBm/Hz. Over the cable, two scenarios model the coexistence with alien DSL services: *i) moderate crosstalk:* AWG thermal noise with spectral density equal to -140 dBm/Hz plus 10 ISDN, 10 ADSL, 4 HDSL, and 2 T1 services; *ii) severe crosstalk:* 20 VDSL disturbers are included in addition to the moderate crosstalk scenario.

The probability density functions for signal power γ_{U_i} and interference terms $\gamma_{U_{j\neq i}}$ and γ_{BS} are shown in Fig. 2 for the case of network MIMO with LMMSE weight matrix $\mathbf{W}_k$ in (7) and for the cable-MMSE case. Fig. 3 and 4 illustrate the performance in terms of the average per-user throughput evaluated according to the RAN4 approach for link-to-system mapping as specified in [9] (maximum spectral efficiency is here 4.4bit/s/Hz). Fig. 3-(a) and (b) show the average per-user LTE uplink throughput versus the macrocell BS distance $D_{BS\to R_i}$ for the moderate and severe alien crosstalk scenario, respectively, with $g_{\text{Wall}} = 5$dB. Short (circle markers), medium (square markers) and long (triangular markers) cable ranges have been considered. The propagation environment is taken from the 2.4GHz layout measurements in fig. 1. The uplink linear processing accounting for the whole air+cable chain according to (7) (solid lines) delivers the maximum benefits in low cross-tier interference regime (say for $D_{BS\to R_i} > 50$m), where throughput is as high as 30 and 18Mbit/s for short cable ranges affected by moderate and severe crosstalk noise, respectively. In a dense femtocell deployment, pure cable-MMSE (dashed lines) without any co-tier radio interference management cannot achieve the FemtoWoC throughput for any scenario. Fig. 4-(a) and (b) show the average per-user LTE uplink throughput versus the penetration loss g_{Wall} ($g_{\text{Wall}} < 10$dB represents a densely deployed scenario). System parameters are the same as in Fig. 3, now with $D_{BS\to R_i} = 60$m. Compound wireless and cable MIMO processing at the receiver (solid lines) delivers up to 30Mbit/s throughput for a short cable range (Fig. 4-(a)), with an almost twofold increase with respect to the cable-MMSE case. Medium and long cable loops paired with severe crosstalk over the cable (Fig. 4-(b)) limit the multicell processing gain for penetration losses greater than 20dB.

A. Channel out-dating effects

The aim of this section is to evaluate the impact of the radio channel out-dating effect as detailed in Sec. IV-A on the system performance. Towards this goal, we consider the case $\rho_{U_i\to R_j} = \rho$, for each $i, j = 1, ..., M$ (channel out-dating is equivalent for all the links $U_i \to R_j$). Moreover, we assume that pilot signals are arranged according to a regular grid over the time-frequency domain, so that, for each carrier, pilot tones periodically occur at time distance $d \times T_b$, being T_b the OFDM symbol duration (here $T_b = 100\mu$s), and d the distance (in number of OFDM symbols) between two

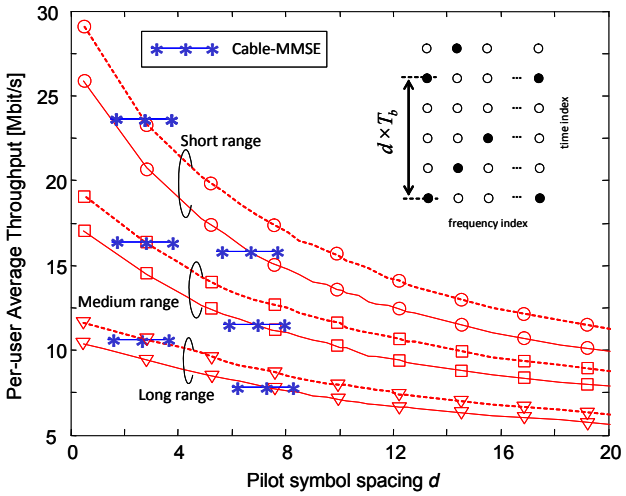

Fig. 5: Average per-user LTE uplink throughput achievable by employing the network MIMO paradigm versus the pilot spacing d. Same legend and parameters as in fig. 4, with $g_{Wall} = 5$ (solid lines) and 15 dB (dashed lines).

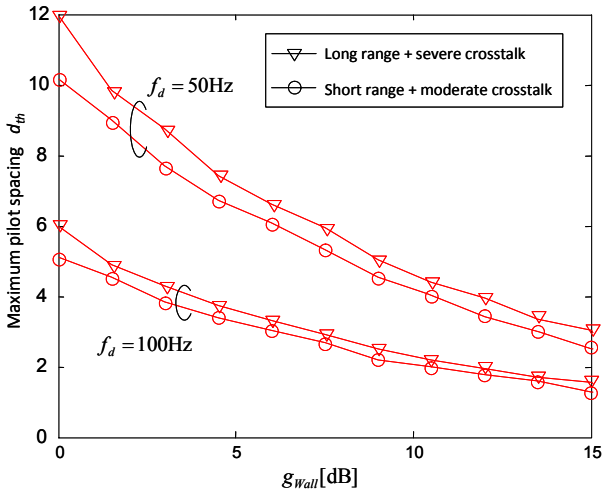

Fig. 6: Maximum allowed pilot spacing d_{th} below which the network MIMO scheme outperforms the cable-MMSE versus the wall penetration loss g_{Wall}, for Doppler shifts $f_d = 50$Hz and $f_d = 100$Hz.

successive training phases, or pilot spacing. Pilot and data subcarriers are transmitted with the same power (equal to P_T).

Fig. 5 shows the average per-user LTE uplink throughput achievable by employing the LMMSE weight matrix (7) versus the pilot symbol spacing d (assumed continuously varying), for short (circle markers), medium (square markers) and long (triangular markers) cable ranges, and for wall penetration losses $g_{Wall} = 5$ (solid lines) and $g_{Wall} = 15$ dB (dashed lines). A severe crosstalk scenario has been considered, while other system parameters are selected as in fig. 4. To model the out-dating of the channel state, the auto-regressive model (8) is adapted to a Clarke model [11], with maximum Doppler shift $f_d = 50$Hz to represent a worst-case scenario with quasi-static indoor terminals [7]. The achievable throughputs for the cable-MMSE are also shown for comparison (lines with star markers). We assume as best case that these are not influenced by the imperfect channel knowledge. Providing an accurate channel estimation from training becomes crucial when coupling effects within both the air and the cable links increase. To improve estimation accuracy, the interval between training symbols should be reduced accordingly. Fig. 6 refers to the same system settings as fig. 5, and shows the maximum allowed pilot spacing value d_{th} below which the network MIMO scheme outperforms the cable-MMSE versus the wall penetration loss g_{Wall}, for Doppler frequencies $f_d = 50$Hz and $f_d = 100$Hz. In each case, two opposite representative scenarios have been selected: short cable range with moderate crosstalk (line with circles), and long cable range with severe crosstalk (line with triangles). For a densely-deployed scenario ($g_{Wall} = 5$dB) with a worst-case Doppler shift ($f_d = 100$Hz) and with severe alien crosstalk over the cable infrastructure, a pilot spacing of $d_{th} = 3$ OFDM symbols is enough to fully exploit the benefits of the FemtoWoC architecture.

VI. Conclusions

The FemtoWoC architecture exploits the benefits of network MIMO in femtocell systems and has been tested using realistic indoor channel measurements. Wireless impairments over the femtocell indoor environment (co/cross-tier interference) are modeled by Rician fading originated by the static multi-path fading component over the short-range indoor links. By mitigating the Rician distributed interference, the FemtoWoC architecture effectively delivers the advantages of distributed antenna systems to the femtocell environment (with up to three-times throughput gains). An accurate design of the pilot spacings for channel estimation is mandatory to balance any performance degradation at the remote multicell FAP.

References

[1] D. Gesbert et al., "Multi-Cell MIMO Cooperative Networks: A New Look at Interference," *IEEE Journal on Sel. Areas in Comm.*, vol. 28, no. 9, Dec. 2010.

[2] J. Gambini, U. Spagnolini, "Radio over Telephone Lines in Femtocell Systems," *21st IEEE Int. Symp. on Personal, Indoor and Mobile Radio Comm.*, pp. 1544-1549, 26-30 Sept. 2010.

[3] C. Oestges et al. "Experimental characterization and modeling of outdoor-to-indoor and indoor-to-indoor distributed channels," *IEEE Trans. Vehicular Tech.*, vol. 59, no. 5, pp. 2253-2265, Jun. 2010.

[4] ITU-T Rec. G.996.1, "Test Procedure for Digital Subscriber Line (DSL) Transceivers," Jun. 1999.

[5] W. A. Porter, S. C. Kak, *Advances in Communications and Signal Processing*. Springer-Verlag, Berlin/Heidelberg, 1989.

[6] P. Kyosti et al., "WINNER II Channel Models," European Commission, Sep. 2007. [Online]. Available: http://projects.celtic-initiative.org/winner+/WINNER2-Deliverables/D1.1.2v1.1.pdf.

[7] S. Savazzi and U. Spagnolini, "Optimizing training lengths and training intervals in continuous time-varying fading channels," *IEEE Trans. On Signal Processing*, pp. 1098-1113, vol. 57, no. 3, March 2009.

[8] ITU-T Rec. G.993.1, "Very-high-speed Digital Subscriber Line (VDSL) Transceiver," Jun. 2004.

[9] Femto Forum White Paper, "Interference management in OFDMA femtocells," March 2010.

[10] Jonathan Gambini, U. Spagnolini, "LTE Femtocell System Through Amplify-and-Forward Over Cable Links," *IEEE Global Comm. Conf., GLOBECOM 2010*, pp. 716-720, 6-10 Dec. 2010.

[11] K. E. Baddour and N. C. Beaulieu, "Autoregressive modeling for fading channel simulation," *IEEE Trans. Wireless Commun.*, vol. 4, no. 4, pp. 1650–1650, Jul. 2005.

[12] A. Abdi and M. Kaveh, "A space-time correlation model for multielement antenna systems in mobile fading channels," *IEEE Journal on Selected Areas in Communications*, vol. 20, no. 3, Apr. 2002.